JOURNAL OF COMPUTATIONAL PHYSICS **127,** 299–308 (1996)
ARTICLE NO. 0176

Artificial Viscosity Models for Vortex and Particle Methods

G.-H. COTTET

LMC-IMAG, Université Joseph Fourier, BP 53, 38041 Grenoble Cédex 9, France

Received September 22, 1995; revised March 7, 1996

The analysis of the truncation error produced by particle methods leads to artificial viscosity schemes. For vortex methods, they can be seen as eddy viscosity models, with anisotropic non-linear diffusion tensors. Numerical experiments on decaying incompressible 2D turbulence illustrate the efficiency of the method, and in particular the fact that the diffusion stops acting in large coherent eddies. For compressible flows, this approach allows us to understand the oscillations produced by particle methods and to derive new artificial viscosity schemes.

1. INTRODUCTION

Vortex methods provide convenient algorithms for the simulation of inviscid or high Reynolds number flows [3, 8]. They consist in concentrating the vorticity field on a discrete number of particles which evolve with the local velocity of the flow computed in a self-consistent way. Diffusion is handled by either adding a random walk to this deterministic motion, or by exchanging vorticity between nearby particles [3, 5]. For inviscid flows, their main characteristics is that they do not introduce numerical diffusion and are quite robust in the sense that they do not suffer time step limitations usually found in grid-based discretizations of advection problems.

Vortex methods are therefore a natural tool to investigate the main features of two-dimensional incompressible turbulence, in particular the mechanisms through which small scales organize themselves into large eddies. Vortex calculations focusing on this problem, starting from an initially chaotic vorticity field, were reported in [7]. It was observed that very soon the results diverge from those obtained by high resolution pseudo-spectral calculations at high Reynolds numbers and that the merging of small eddies could not be satisfactorily achieved by vortex methods. We will show results later which confirm this conclusion.

Our primary goal here is to understand how the truncation error in vortex methods can be responsible for this failure and, then, to propose optimal correction terms to overcome these difficulties. By optimal we mean that we will seek corrections which will act only when and where needed, as opposed to Navier–Stokes models which eventually completely dissipate the vorticity field.

It turns out that the precise form of the error produced by vortex methods, and not only their order of convergence, can be precisely analyzed. This feature, which definitely distinguishes vortex methods from grid-based methods, stems from the fact that vortex methods and, more generally, particle methods are based on *exact* weak solutions of advection equations. The truncation error solely results from the mollification used in practice in the computations of the particle's velocity. This mollification introduces a cutoff in the short-range interactions of particles. If we denote by u and ω the velocity and vorticity fields and by $\bar{u}, \bar{\omega}$ the mollified fields, the truncation error involves the tensor

$$\overline{\bar{u}\omega} - \bar{u}\omega \tag{1}$$

Not surprisingly, this tensor is reminiscent to the $u\omega - \bar{u}\bar{\omega}$ tensor which is (in a velocity–vorticity formulation) the starting point of all eddy viscosity models. However, it turns out that (1) shares with the so-called Leonard stress tensor $\overline{\bar{u}\bar{\omega}} - \bar{u}\bar{\omega}$ the nice feature that no closure model is required to express it, at the leading order, in terms of the resolved scales. Straightforward asymptotic expansions actually lead to a differential operator in $\bar{\omega}$, the order of which is related to the moment properties of the mollifying function.

Our approach will then significantly differ from the one used in the derivation of the sub-grid models used in general in the context of finite-differences or spectral large eddy simulations. These methods are related to eddy viscosity models through the assumption that the numerical schemes compute some kind of average of the solution, on a gridsize scale, and thus must be based on the filtered Navier–Stokes equations. We will instead start from the equivalent equation satisfied by vortex schemes and try to correct it in order to reproduce the large eddy dynamics expected for the original, and not the filtered, Euler equations. As a matter of fact, that our corrections are of the order of the mollifying function suggests that sub-grid models, which are all based on second-order diffusion terms, might be too dissipative if used together with high order discretizations of the equations. In other words, we believe

0021-9991/96 $18.00

that sub-grid models should not be derived independently of the choice of numerical method.

There are two additional features of our model that we wish to emphasize. It is anisotropic by essence, and, unlike Smagorinsky type models, does not introduce unwanted dissipation in the core of coherent eddies. From this point of view our work is connected to two general issues raised by LES models, namely the possible improved efficiency offered by anisotropic models and the need, pointed out in recent LES research [9], to compute diffusion coefficients after filtering out the largest scales of the fields to avoid dissipation in the large eddies.

The derivation of an equivalent equation is also the key ingredient to understand convergence properties of particle methods for compressible flows. Arguments based on similar expansion, as for vortex methods, allow us to understand the oscillations resulting around shocks from a naive implementation of particle methods and to propose optimal artificial viscosity models.

The paper is organized as follows. Sections 2 to 5 deal with vortex methods. The truncation error is analyzed in Section 2 and interpreted in Section 3, and the eddy viscosity model is derived in Section 4. Section 5 is devoted to numerical results. We address the case of compressible flows in Section 6 and draw some conclusions in Section 7.

2. TRUNCATION ERROR ANALYSIS FOR 2D VORTEX METHODS

Vortex methods are based on the velocity–vorticity formulation of the incompressible Euler equations which in 2D read

$$\frac{\partial \omega}{\partial t} + \operatorname{div}(u\omega) = 0 \tag{2}$$

$$\operatorname{curl} u = \omega; \quad \operatorname{div} u = 0; \quad u \to u_\infty \quad \text{at infinity.} \tag{3}$$

They consist in approximating the initial vorticity field ω_0 by a set of particles

$$\omega_0(x) \simeq \omega_0^h(x) = \sum_p \alpha_p \delta(x - x_p). \tag{4}$$

The strength α_p of particle p is the local circulation at x_p, which can be represented as the product of the local value of the vorticity ω_p by the volume v_p around the particle x_p.

Conservation of the circulation dictates that particles will move with the local velocity of the flow and conserve their strength. In other words the vorticity field generated by ω_0^h is, at all times, given by

$$\omega^h(x,t) = \sum_p \alpha_p \delta(x - x_p(t)). \tag{5}$$

Note that, since the flow is incompressible, volumes and vorticity values are conserved as well along the particle trajectories. The fact that (5) gives the actual solution to (2) is the very basic feature of the vortex method, on which all the foregoing analysis will be based. It can be phrased in precise mathematical terms in the framework of weak measure solution to advection equations [4].

In writing (5), we have, however, assumed that the velocity field was given. We must account for the fact that it is coupled to the vorticity field through (3), or, equivalently, the Biot–Savart law,

$$u = u_\infty + K * \omega. \tag{6}$$

The kernel K has a singularity at the origin which it is customary to remove via the convolution by a mollifying function. The resulting vortex blob method—to refer to the fact that particles are replaced by finite size blobs for the computation of the velocity—can be summarized by

$$\frac{\partial \omega^h}{\partial t} + \operatorname{div}(u_\varepsilon \omega)^h = 0, \tag{7}$$

$$u_\varepsilon = K_\varepsilon * \omega^h, \tag{8}$$

where

$$K_\varepsilon = K * \zeta_\varepsilon$$

and the function ζ_ε is obtained from a cutoff function ζ by the following scaling:

$$\zeta_\varepsilon(x) = \varepsilon^{-2}\zeta(x/\varepsilon). \tag{9}$$

We will assume in the sequel that ζ has radial symmetry and mean value 1:

$$\zeta(x) = f(|x|); \quad \int \zeta(x)\,dx = 1. \tag{10}$$

These conditions lead to at least order 2 approximations. Additional moment properties of ζ yield higher order approximations. We refer to [2, 1, 4] for more complete discussions and analysis of these methods.

One natural candidate to approximate the exact vorticity ω is the smooth approximate vorticity field

$$\omega_\varepsilon = \omega^h * \zeta_\varepsilon. \tag{11}$$

The key point of our analysis will now be to derive the

equivalent equation satisfied by ω_ε. By convolving (7) with ζ_ε we get

$$\frac{\partial \omega_\varepsilon}{\partial t} + \operatorname{div}(u_\varepsilon \omega_\varepsilon) = E, \tag{12}$$

where the truncation error E results from the fact that, in the nonlinear term in the left-hand side, we only applied the convolution on ω; so, if for simplicity we drop the variable t,

$$E(x) = \operatorname{div}_x \int \omega(y)[u_\varepsilon(x) - u_\varepsilon(y)]\zeta_\varepsilon(x-y)\,dy. \tag{13}$$

To better interpret this term, it is convenient to split it into two terms by writing $\omega(y) = \omega(x) + (\omega(y) - \omega(x))$; we obtain

$$E = E_1 + E_2,$$

where

$$E_1(x) = \operatorname{div}_x \left(\omega(x) \int [u_\varepsilon(x) - u_\varepsilon(y)]\zeta_\varepsilon(x-y)\,dy \right) \tag{14}$$

$$E_2(x) = \operatorname{div}_x \int [\omega(y) - \omega(x)][u_\varepsilon(x) - u_\varepsilon(y)]\zeta_\varepsilon(x-y)\,dy. \tag{15}$$

The first term E_1 is a drift term which can be rewritten as

$$E_1 = \operatorname{div}(\tilde{u}_\varepsilon \omega), \tag{16}$$

where $\tilde{u}_\varepsilon$ is a divergence-free vector field. In particular, it does not contribute to any enstrophy variation and we will not consider it further at this time.

Let us focus on E_2. To have a better understanding of the nature of this error term it will be worthwhile to assume momentarily that we deal with a non-negative cutoff function. A Taylor expansion of ω and u_ε inside the right-hand side of (15) yields

$$\begin{aligned} E_2(x) = \operatorname{div}_x \sum_{i,j} \int & [(y_i - x_i)\partial_i u_\varepsilon(x)] \\ & [(x_j - y_j)\partial_j \omega(x)]\zeta_\varepsilon(x-y)\,dy \\ & + O\left(\int |x-y|^4 \zeta_\varepsilon(x-y)\,dy \right). \end{aligned}$$

But, due to the radial symmetry of ζ_ε, the cross terms $\int [(y_i - x_i)][(x_j - y_j)]\zeta_\varepsilon(x-y)\,dy$ vanish for $i \neq j$ so that rearranging the derivatives and using a straightforward change of variables in the integrals give

$$E_2 = m_2 \varepsilon^2 \operatorname{div}([Du_\varepsilon]\nabla\omega) + O(\varepsilon^4), \tag{17}$$

where

$$m_2 = \frac{1}{2} \int |x|^2 \zeta(x)\,dx \tag{18}$$

and $[Du_\varepsilon]$ is the tensor $(\partial(u_\varepsilon)_i/\partial x_j)$. Note that the assumption on the positivity of ζ was only made to make sure that m_2 is non-zero. We will come back to this point later.

Similar calculations can be found in [8], leading, however, to a diffusion tensor written in a non-conservative form. Technically, splitting E into $E_1 + E_2$ and obtaining E_2 in a conservative form will help us in the forthcoming discussion. Let us also mention that similar expansions allow us to obtain the following expression for the drift term E_1,

$$E_1 = -m_2 \varepsilon^2 \operatorname{div}(\omega \operatorname{curl} \omega) + O(\varepsilon^4).$$

3. INTERPRETATION OF THE TRUNCATION ERROR

We now come to the discussion of the effect of the error term E_2 on the dynamics of the flow as computed by vortex methods. We still focus in this section on the case of a positive cutoff.

One important issue concerning E_2 is to understand its diffusive or antidiffusive nature. Starting from (17), one natural way to address this issue is to think of the tensor $[Du_\varepsilon]$ in diagonal form: positive (resp. negative) eigenvalues will induce antidiffusion (resp. diffusion) along directions parallel to the corresponding eigenvectors. A first obvious remark is that, due to the incompressibility of the flow, the trace of this tensor is zero. As a result any diffusion will be balanced by antidiffusion in a complementary direction. This confirms the fact, already attested by the conservation of energy resulting from the hamiltonian form of the dynamical system driving the motion of particles, that vortex methods do not produce net numerical diffusion, as would most eulerian methods.

However, this balance of diffusion and antidiffusion does not necessarily mean that vortex methods will correctly reproduce the features of inviscid 2D flows. To substantiate this claim, we have performed calculations based on the same initial conditions as in [7]. We start from an initial vorticity with, in the Fourier space, a spectral law in k^{-1} and random phase. This field is normalized to have a maximum vorticity value of 1. We then interpolate this field on a particle mesh initialized uniformly on the unit square. To handle periodic boundary conditions in a simple and fast way, the velocity calculations are done through a vortex-

FIG. 1. Vorticity values at $t = 20$ and $t = 60$ for a pure Euler scheme (bottom pictures) and the eddy viscosity model (top pictures).

in-cell scheme. In this method, at each time step the circulations of the particles are projected on a fixed regular grid; then a fast Poisson solver is called to compute the stream function on this grid. Finite differences are used to get velocity values at the grid points. Finally velocities are interpolated from the grid to the particles. Although in practical implementation this scheme clearly differs from the completely grid-free one outlined in the previous section, we believe that the truncation mechanisms are similar, with the interpolating function playing the role of the cut-off function.

The two bottom pictures of Fig. 1 show, in grey levels, the vorticity fields at times 20 (left picture) and 60 (right picture). The finite-difference grid for the velocity calculation is 64×64. To have a good overlapping of particles, at least at $t = 0$, the particle mesh is 128×128. One observes that, in the first picture, small scales tend to organize into filaments and large eddies. However, this merging process does not completely succeed, and, at later times, the flow tends to a complete mixing of positive and negative vorticity, and all the coherent eddies disappear (one can still guess them in the right picture, but the mixing is actually achieved soon afterwards).

Another illustration of the same mechanisms can be found in the vortex sheet calculations [6]. In this case, although the flow is much better organized by the selection of one particular perturbation, small eddies excitated at late times by roundoff errors have to be filtered out in order to avoid spurious effects on the large eddies. We will also see in Section 5 that to some extent remeshing the particle grid is, besides filtering, one way to handle small scales.

The eddy viscosity scheme that we will derive is based on the claim that the antidiffusive part of E_2 is responsible for the failure of the vortex methods in allowing the merging of small eddies. Before getting to this, let us now discuss further the tensor in the right-hand side of (17). Let us split the velocity derivatives into strain and vorticity. With the notations:

$$s_1 = \frac{\partial u_1}{\partial x_1} - \frac{\partial u_2}{\partial x_2}; \quad s_2 = \frac{\partial u_2}{\partial x_1} + \frac{\partial u_1}{\partial x_2};$$

since div $u = 0$, we can write

$$[Du] = \frac{1}{2}\begin{bmatrix} s_1 & s_2 - \omega \\ s_2 + \omega & -s_1 \end{bmatrix}.$$

The determinant of this matrix is $(\omega^2 - |s|^2)/4$. As a result, it has real eigenvalues as soon as the strain $|s| = \sqrt{s_1^2 + s_2^2}$ is larger than the absolute vorticity. The corresponding zones are called hyperbolic, to refer to the trajectories around saddle-points (a typical such configuration is at a stagnation point in a potential flow). From our analysis strong diffusion and antidiffusion are very likely to be produced by vortex methods in such parts of the flow.

4. THE EDDY VISCOSITY MODEL

As we said above, we believe that, in order to reproduce the basic features of 2D turbulence, it is important to prevent the antidiffusive mechanisms embedded in the error term E. To derive our model, since clearly we cannot afford to diagonalize the error tensor and explicitly correct the positive eigenvalue, we propose to go back to the integral form of the equivalent equation, with the error term written in (13), and to evaluate the enstrophy production based on this equation. Any positive production of enstrophy will then be interpreted as the indication of antidiffusivity, and our model will be designed to compensate for this enstrophy production.

Let us now get into the details of the derivation. We first observe that, to the leading order, we may replace ω by ω_ε in (13). We then multiply (13) by ω_ε and integrate by parts. Dropping everywhere the subscript ε for clarity, we obtain

$$\frac{1}{2}\frac{d}{dt}\int \omega^2\,dx = \int\int \omega(x)\omega(y)[u(x) - u(y)] \cdot \nabla\zeta(x - y)\,dx\,dy. \tag{19}$$

We next rewrite $\omega(x) = \omega(y) + \omega(x) - \omega(y)$ to get

$$\frac{1}{2}\frac{d}{dt}\int \omega^2\,dx = \int\int \omega^2(y)[u(x) - u(y)] \cdot \nabla\zeta(x - y)\,dx\,dy + \int\int [\omega(x) - \omega(y)]\omega(y)[u(x) - u(y)] \cdot \nabla\zeta(x - y)\,dx\,dy.$$

The first integral in the right-hand side above vanishes, for $\omega(y)$ can be put out of the integral with respect to x and

$$\int [u(x) - u(y)] \cdot \nabla\zeta(x - y)\,dx = -u(y) \cdot \int \nabla\zeta(x - y)\,dx + \int \mathrm{div}_x[u(x)\zeta(x - y)]\,dx = 0.$$

We are left with the second integral, which, upon rewriting $2\omega(y) = [\omega(x) + \omega(y)] - [\omega(x) - \omega(y)]$ and using the parity of ζ yields

$$\frac{d}{dt}\int \omega^2\,dx = -\int\int [\omega(x) - \omega(y)]^2[u(x) - u(y)] \cdot \nabla\zeta(x - y)\,dx\,dy. \tag{20}$$

Note that we would have obtained the same result if we had started from E_2. We have actually checked on the integral exact form of E that the term E_1 does not contribute to enstrophy production. The interpretation of (20) is now clear: the enstrophy will increase through the exchange of vorticity between points x and y whenever they satisfy

$$[u(x) - u(y)] \cdot \nabla\zeta(x - y) < 0. \tag{21}$$

If we consider one more time the particular case of a positive cutoff decaying at infinity and with radial symmetry then $\nabla\zeta(z) = zf'(|z|)/|z|$ with $f' \le 0$, so that (21) is equivalent to

$$[u(x) - u(y)] \cdot (x - y) > 0. \tag{22}$$

This confirms in particular the fact, predicted from the asymptotic expansions of Section 3, that if the velocity is generated by a steady circular patch of vorticity (zero strain) then there is neither diffusion nor antidiffusion.

Now, a *minimal* artificial viscosity model must precisely cancel the enstrophy production arising under condition (21). To achieve this goal, the proper vortex scheme consists in updating the vorticity values at the particle locations through

$$\frac{d\omega_p}{dt} = \sum_q (\omega_p - \omega_q)v_q\{[u(x_p) - u(x_q)] \cdot [x_p - x_q]f'_\varepsilon(|x_p - x_q|)|x_p - x_q|^{-1}\}_-, \tag{23}$$

where the index $-$ means that we take the negative part of the quantity and we recall that ω_p and v_p respectively denote the vorticity value and the volume of the particle located at x_p. Indeed, multiplying (23) by $v_p\omega_p$, summing over p, and using symmetry properties yield

$$\frac{d}{dt}\left(\sum_p v_p|\omega_p|^2\right) = \sum_{p,q} v_p v_q(\omega_p - \omega_q)^2\{[u(x_p) - u(x_q)] \cdot [x_p - x_q] f_\varepsilon'(|x_p - x_q|)|x_p - x_q|^{-1}\}_-$$

which is the appropriate cancellation, at the discrete level (through quadrature of the integrals over particles), of the enstrophy production resulting from (20).

The diffusion scheme given by (23), which is reminiscent of particle strength exchange methods [5], is clearly conservative. If $f' \leq 0$ exchange of vorticity will only concern diverging particles. As a result, if the velocity field is generated by a circular patch of vorticity, there will never be any exchange of vorticity between particles, even if there is a strong gradient of vorticity inside the patch. This contrasts with Smagorinsky-type models, which would produce strong diffusion in the same situation.

In closing this section we wish to emphasize that the above derivation did not rely on the asymptotic expansions of the last sections, since it is based on the integral form of the error term. In particular it applies to high order cutoff, in which case it provides hyperviscosity-type models. Next, the fact that the scheme (23) is by essence anisotropic, as it distinguishes for the diffusion among directions of compression and dilatation, illustrates the flexibility of particle strength exchange schemes in handling diffusion: the particle mesh allows us to discretize more directions than a grid-based method.

5. NUMERICAL RESULTS

We first focus on the periodic decaying turbulence experiments already mentioned in Section 2. Our computations are based on the same 64×64 vortex-in-cell scheme. To implement our diffusion scheme (23), we used the hat function as cutoff ζ, normalized such that it has the same order 2 momentum as the piecewise quadratic TSC interpolation function.

The two top pictures of Fig. 1 show that vorticity values at the same times as the bottom pictures. We observe that the coherent eddies do appear, organized either in filaments or in patches. We wish to point out that, if a finer grid was used, like the one in the next experiment, the pure Euler model would take more time to fail and actually would provide results very close to the bottom pictures for early times. This is coherent with our analysis, which shows that truncation errors are driven by the grid resolution and not by the overlapping of blobs.

The key point is now to compare this method to a standard linear artificial viscosity model. In Fig. 2 we show results obtained with the VIC method, with a 128×128 grid and a particle mesh of 256×256. The right picture depicts the vorticity field at time 160, for a Navier–Stokes model with viscosity $\nu = 10^{-5}$, which is about the minimal

FIG. 2. Comparison of the eddy viscosity model and a pure Navier–Stokes model.

viscosity allowed by the resolution of the grid. The left picture shows the corresponding vorticity fields obtained with the model (23). It can be observed that the filaments are better preserved with our model, which presumably diffuses along rather than across them. Also the enstrophy level is about 20% higher for the left vorticity field (this is not apparent in the pictures, which for better clarity use renormalized vorticity values), which confirms that our model is less dissipative than the Navier–Stokes model, although the strength of the "equivalent" viscosity produced by (23) can be locally significantly bigger (in the regions of high strain) than the value of ν used in the Navier–Stokes experiment.

The next experiment precisely aimed at evaluating this local equivalent viscosity $\nu(x)$, which, on the basis of the analysis in Section 2, we measured as

$$\nu(x) = m_2\varepsilon^2 \sup_y \frac{[[u(x) - u(y)] \cdot [x - y]]_+}{|x - y|^2}.$$

For the same parameters as for the previous experiment, the left pictures of Fig. 3 show the vorticity fields at time 60 and 120, and the right ones picture the values of ν encoded such that large viscosity appears in white. The correlation between the flow patterns and viscosity values is striking. It is in particular clear that the regions of strong viscosity coincide in the top pictures with the saddle-points in between the two big eddies which will ultimately lead to a steady-state dipole. This confirms the analysis of the error term E in terms of the strain in the flow.

We just mentioned that the flow goes toward a steady state. To substantiate this claim we show in Fig. 4 the vorticity at some later time and the scatter plot obtained by plotting for each grid point the coordinates corresponding to the value of the stream function and of the vorticity. These values are concentrated around a curve, $\omega = g(\psi)$, which indicates that we are not far from a steady-state solution.

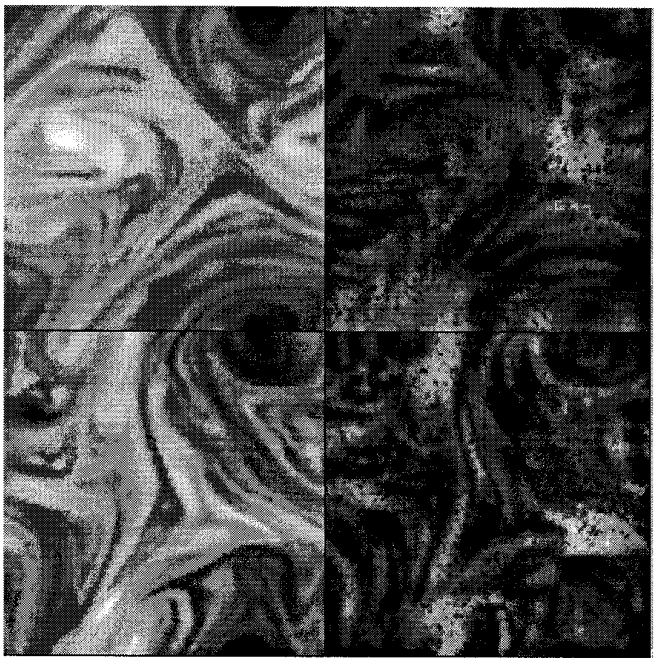

FIG. 3. Correlations between the flow patterns (left pictures) and the strength of the diffusion tensor (right pictures) at times 60 and 120.

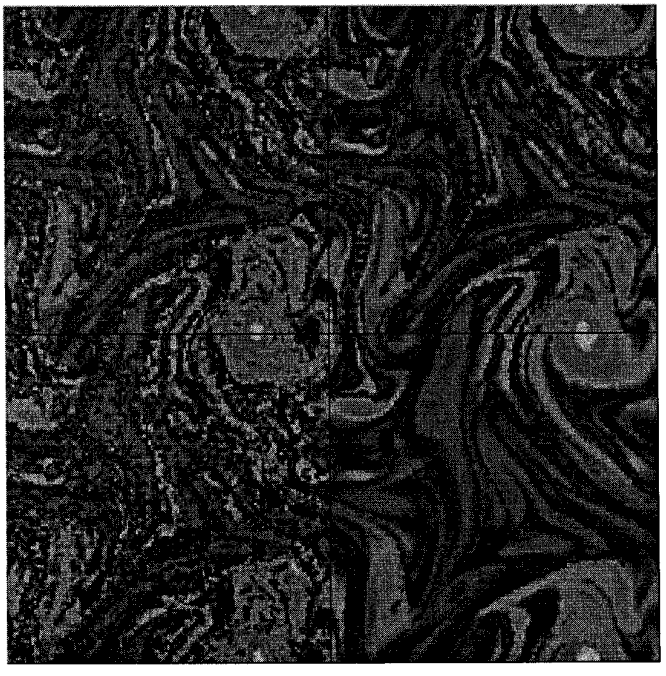

FIG. 5. Comparison of the eddy viscosity model (bottom-right) and the pure Euler model with 0 (bottom-left), 1 (top-left), and 2 (top-right) remeshings.

We next wanted to compare the effect of our eddy viscosity model and that of remeshing. One can actually advocate that the reason for the vortex method to fail in a pure Euler model is that the grid mesh gets very strongly distorted and, thus, does not allow the accurate description of the flow. In particular, the overlapping between blobs which is required for the convergence of the method is soon violated. The goal of remeshing is to recover a regular grid at selected times of the computation.

Technically, remeshing amounts to interpolating vorticity values from one grid to another. The choice of the interpolation function is crucial to keep as small as possible the discrepancies between the vorticity field before and after remeshing. In general, the conservation of Euler invariants, like total vorticity and linear and angular impulse, is sought in order to make sure that remeshing does not introduce too much dissipation. However, our experience on this particular type of flow was that it was necessary to have a slightly dissipative remeshing procedure to avoid introducing even more noise in the already nonsmooth vorticity field. In the computations we present, we have used the TSC interpolation function and, when remeshing, we not only recompute vorticity values on a regular grid of grid size h, but also volumes of the particles which can slightly differ from h^2.

In Fig. 5, we reproduce on the bottom pictures the vorticity fields at time 60, obtained by the Euler and the eddy viscosity model. The top pictures show the vorticity values obtained when the particles were remeshed once (at time 20) for the left picture, or twice (at times 20, 40) for the right picture. In the last case, the results are very close to those obtained by the eddy viscosity model, apart from a more noisy look of the filaments, and the fact that the enstrophy level of the remeshed field is higher than or the eddy viscosity model (this explains why the grey levels are not identical on both images). If one believes that the remeshed calculation gives the ''true'' solution of the Euler equations, at this low resolution, one can conclude that, up to minor details, the eddy viscosity models preserved rather well the features of the flow.

As a last illustration of our method, we performed some numerical tests with high order cutoff. In this case we use the plain vortex blob method (with a grid-free evaluation

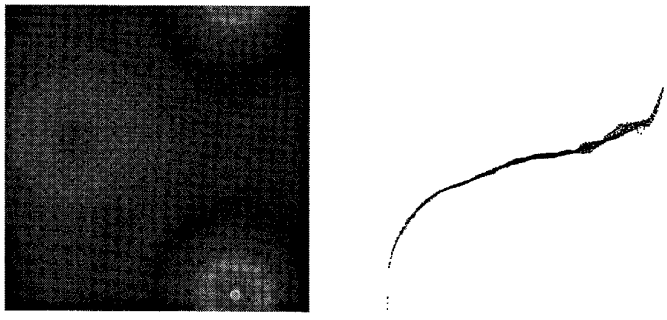

FIG. 4. Vorticity and scatter plot $\psi - \omega$ at late time.

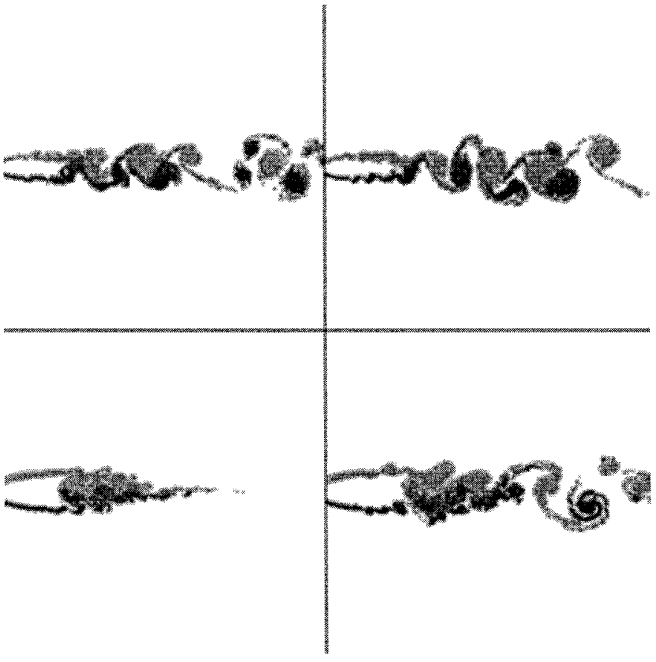

FIG. 6. Vortex street resulting from the merging of two shear layers.

of the velocities). The physical case we had in mind was a jet consisting of two shear layers of opposite strength. The shear layers are separated upstream by a fixed distance to mimic the wake behind an obstacle. The parameters of the problem were the following: the distance between the shear layers was 1, the width of each shear layer was 0.05, and the far-field velocity was 1. Each shear layer was discretized with 10 particles in the width, and the generation of particles upstream was such that the average distance of the particles in the direction of the mean flow was about the width of the layers. Finally, we prescribed hyperbolic tangent profiles for the velocity in each layer and we triggered the instability of the shear layers by introducing a small random noise in the strength of the vortices injected upstream.

In Fig. 6 we have represented a sequence of vorticity values (from left to right, bottom to top), showing the merging of small eddies at various scales, leading to a vortex street consisting of rather well-organized dipoles. At the last stages of the calculation there were about 15,000 particles. Due to the random forcing introduced at the injection of the particles, it is rather difficult to compare results obtained with different parameters or different simulation methods. The only comment we wish to make on these simulations is that we never used any remeshing and that, in the same conditions, we were not able to keep an organized vortex street for such a long time with a Navier–Stokes code using a viscosity value of the order of ε^2.

6. COMPRESSIBLE FLOWS

We will now see how the same strategy as above allows us to derive artificial viscosity models for the particle approximation of compressible flows. We will focus on the very basic 1D model for such flows, namely Burger's equation,

$$\frac{\partial u}{\partial t} + \frac{1}{2}\frac{\partial (u^2)}{\partial x} = 0. \tag{24}$$

The naive way to construct particle methods for this equation is to replace the initial value of u by a set of particles that will move with the local velocity field. Although this field can develop discontinuities, it is important to have a well-defined motion of the particles. This can be done again by regularizing the velocity, either through the interpolation of particle values on a grid (the so-called PIC methods), or through the direct convolution of the particle distribution with a cutoff function.

Our motivation in the incompressible case was to reproduce some fine features of the Euler equations. Here we will be much less ambitious; actually some very important steps in the calculations of Sections 2 to 4 were heavily based on the fact that the velocity field was divergence-free. Our goal here is only to try to understand the convergence of particle methods. It is actually striking that, to our knowledge, no convergence proof exists even in the very simple situation just described. The reason is that, if for a given regularization parameter ε one lets the number of particles tend to infinity, the best one can hope is to converge to the solution of the equation

$$\frac{\partial u}{\partial t} + \frac{1}{2}\frac{\partial (u_\varepsilon u)}{\partial x} = 0. \tag{25}$$

It turns out that this equation is not well behaved as ε tends to 0. The only control one can get on its solution, uniformly with respect to ε, is the mean value of u. In particular it is not possible to obtain any maximum principle or even any control on its energy. As a matter of fact, one can easily understand how a simple-minded implementation of the method leads to overshoots around shocks; at a steady shock, the mollified velocity is 0, so particles will accumulate from both sides and lead to large local values of u.

Let us derive an equivalent equation for (25). This equation will lead us to the proper artificial model to ensure the decay of energy.

If we assume momentarily that

$$u_\varepsilon = u * \zeta_\varepsilon; \quad \zeta_\varepsilon = \varepsilon^{-1}\zeta(x/\varepsilon),$$

where ζ is a positive even cutoff, then we can write

$$u_\varepsilon = u + m_2\varepsilon^2 u_{xx} + O(\varepsilon^4), \tag{26}$$

where $m_2 = \int x^2\zeta(x)\,dx$. Upon inserting (26) in (25), multiplying it by u, and integrating, we obtain, after cancellation of the contribution of u^2,

$$\frac{d}{dt}\int |u|^2\,dx + \frac{m_2}{2}\varepsilon^2\int (u_{xx}u)_x u\,dx = 0. \tag{27}$$

Successive integrations by parts yield

$$\int (u_{xx}u)_x u\,dx = -\int u_{xx}uu_x = -\frac{1}{2}\int (u_x^2)_x u\,dx$$

$$= \frac{1}{2}\int u_x^2 u_x\,dx.$$

As a result, the increase of energy comes from strong negative values of the velocity gradient, which precisely occurs at shocks. The artificial viscosity model which will prevent it is now clearly

$$u_t + \frac{1}{2}(u_\varepsilon u)_x + \frac{m_2}{4}\varepsilon^2((u_x)_- u_x)_x = 0. \tag{28}$$

The particle discretization of the diffusion term above requires its integral representation. Straightforward asymptotic expansions yield

$$\frac{m_2}{2}\varepsilon^2(au_x)_x = \int a\left(\frac{x+y}{2}\right)(u(y)-u(x))\zeta_\varepsilon(y-x)\,dy + O(\varepsilon^4).$$

If $a = (u_x)_-$ and if, in addition, we write

$$u_x\left(\frac{x+y}{2}\right) \simeq \frac{u(y)-u(x)}{y-x},$$

we obtain

$$u_t + \frac{1}{2}(u_\varepsilon u)_x + \frac{1}{2}\int \left(\frac{u(y)-u(x)}{y-x}\right)_- (u(y)-u(x))\zeta_\varepsilon(y-x)\,dy = 0. \tag{29}$$

It turns out that the decay of energy can directly be checked on the integral form (29) through straightforward algebraic calculations that we do not reproduce here. This means that, again, the asymptotic expansions which led us to (29) are not actually needed for its justification. In particular, (29) is valid even for nonpositive cutoff, in which case it leads to an hyperviscosity model.

The final particle scheme based on (29) is

$$u \simeq \sum_p u_p v_p \delta(x - x_p); \quad \frac{dx_p}{dt} = \frac{1}{2}u_\varepsilon(x_p);$$

$$\frac{dv_p}{dt} = \frac{1}{2}\left(\frac{du_\varepsilon}{dx}(x_p)\right)v_p$$

and

$$\frac{du_p}{dt} = \frac{1}{2}\sum_q v_q\left(\frac{u_p-u_q}{x_p-x_q}\right)_-(u_p-u_q)\zeta_\varepsilon(x_p-x_q). \tag{30}$$

Note that, as for incompressible flows, this model distinguishes between compression and expansion zones, but with the opposite conclusion; dissipation must be added in compression zones.

Numerical tests [11] show that this model is actually able to get rid of overshoots without introducing spreading on the shocks.

This model generalizes easily to several dimensions by splitting the flux and adding the contribution of each direction in the energy balance. In the resulting model one then has to repace u_x by the divergence of u. Our result is then very similar to the artificial viscosity models currently used in SPH methods [10], in particular, in that only approaching particles contribute to dissipation. However, in these models there is in general no explicit reference to any motion regularization, so the parameter ε has to be somehow adjusted to the separation scale of particles; by contrast our model is free of ad-hoc constants and clearly shows the links between the needed amount of viscosity and the regularization introduced in the motion of particles. We will present elsewhere numerical simulations based on (30).

7. CONCLUSION

We have shown that the concept of an equivalent solution is powerful to allow us to derive a nontrivial artificial viscosity model for particle methods. We view this as a consequence of the fact that particle methods are based on exact solutions of advection equations. The error comes from the short-range cutoff needed for evaluating the velocities of particles.

In compressible flows, this error results in oscillations around shocks. The analysis of the equivalent equation sheds some new light on artificial viscosity models currently used in SPH methods and may lead to more efficient models.

For incompressible flows, this analysis allows us to understand the mechanisms which drive vortex simulations

away from the expected dynamics of 2D turbulence and suggests an eddy viscosity model to correct them. This model is anistropic by essence and able to distinguish between vorticity and strain. As a result the added dissipation does not affect large eddies. Our numerical results indicate that simulations using this eddy viscosity model are less sensitive to the usual overlapping condition than purely inviscid or Navier–Stokes models.

However, the real challenge concerns 3D simulations. In 3D flows small scales are constantly excited through stretching and it is crucial to be able to handle these scales. Remeshing and grid refinement at some point most often lead to unaffordable numbers of elements and dissipation mechanisms such as the one we derived in 2D may add some flexibility to vortex schemes. Our future plans consist in incorporating the error coming from the stretching term in the present analysis to derive 3D eddy viscosity models.

REFERENCES

1. C. Anderson and C. Greengard, *SIAM J. Numer. Anal.* **22,** 413 (1985).
2. J. T. Beale and A. Majda, *Math. Comput.* **32,** 29 (1982).
3. A. Chorin, *J. Fluid Mech.* **57,** 785 (1973).
4. G.-H. Cottet, *Ann. Inst. Henri Poincaré* **5,** 227 (1988).
5. P. Degond and S. Mas-Gallic, *Math. Comput.* **53,** 485 (1989).
6. R. Krasny, *J. Fluid Mech.* **167,** 65 (1986).
7. W. D. Henshaw, H.-O. Kreiss, and L. G. Reyna, On the smallest scale estimates and a comparison of the vortex method to the Pseudo-Spectral method, Lectures in Appl. Math., Vol. 28, (Am. Math. Soc., Providence, RI, 1991), p. 303.
8. A. Leonard, *J. Comput. Phys.* **37,** 289 (1980).
9. M. Lesieur and O. Métais, *Annu. Rev. Fluid Mech.* **28** (1996).
10. J. J. Monaghan and R. A. Gingold, *J. Comput. Phys.* **52,** 374 (1983).
11. C. Picard, unpublished.